ACS APPLIED MATERIALS & INTERFACES

Research Article

www.acsami.org

Localized Synthesis of Conductive Copper–Tetracyanoquinodimethane Nanostructures in Ultrasmall Microchambers for Nanoelectronics

Yanlong Xing,[‡,§] Guoguang Sun,[§] Eugen Speiser,[§] Norbert Esser,[‡,§] and Petra S. Dittrich*[,‡,#]

[‡]School of Analytical Sciences Adlershof, Humboldt-Universität zu Berlin, 12489 Berlin, Germany

[§]Leibniz-Institute for Analytical Sciences, ISAS Berlin, 12489 Berlin, Germany

[#]Department of Biosystems Science and Engineering, ETH Zürich, 4058 Basel, Switzerland

Supporting Information

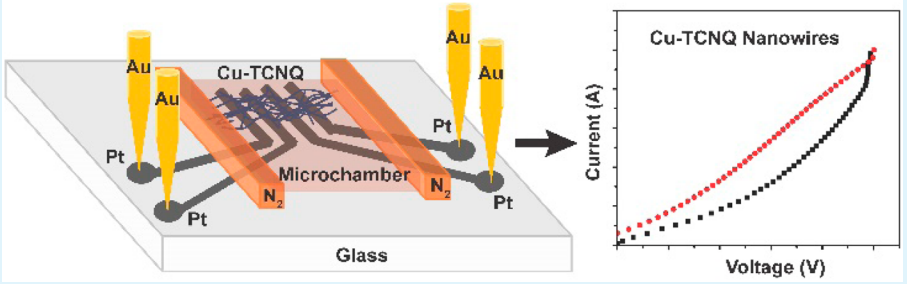

ABSTRACT: In this work, the microfluidic-assisted synthesis of copper-tetracyanoquinodimethane (Cu–TCNQ) nanostructures in an ambient environment is reported for the first time. A two-layer microfluidic device comprising parallel actuated microchambers was used for the synthesis and enabled excellent fluid handling for the continuous and multiple chemical reactions in confined ultrasmall chambers. Different precautions were applied to ensure the reduction state of copper (Cu) for the synthesis of Cu–TCNQ charge-transfer compounds. The localized synthesis of Cu and *in situ* transformation to Cu–TCNQ complexes in solution were achieved by applying different gas pressures in the control layer. Additionally, various diameters of the Cu–TCNQ nano/microstructures were obtained by adjusting the concentration of the precursors and reaction time. After the synthesis, platinum (Pt) microelectrode arrays, which were aligned at the microchambers, could enable the *in situ* measurements of the electronic properties of the synthesized nanostructures without further manipulation. The as-prepared Cu–TCNQ wire bundles showed good conductivity and a reversible hysteretic switching effect, which proved the possibility in using them to build advanced nanoelectronics.

KEYWORDS: *organic electronics, Cu–TCNQ, nanostructures, microfluidics, nanoelectronics*

1. INTRODUCTION

Metal–organic charge-transfer complexes based on 7,7,8,8-tetracyanoquinodimethane (TCNQ) have attracted considerable research interest, due to their intriguing electronic properties and their potential applications in building advanced conductive materials, sensors, and energy and data storage substrates.[1−4] Cu–TCNQ is considered to be representative of complexes with TCNQ because of its reversible, bistable switching capabilities in conductivity when induced by an electric field. The bulk and thin films of Cu–TCNQ have been extensively studied. However, after the discovery of its quasi-one-dimensional (1D) crystalline nanostructures,[5,6] Cu–TCNQ has received greater attention in the nanotechnology field, due to its advantages for building practical nanoelectronics over their bulk and thin film counterparts. For example, He et al. described the use of Cu–TCNQ microribbon electrodes in organic single-crystal transistors.[7] For this reason, various approaches in obtaining Cu–TCNQ nanostructures have been reported, such as chemical vapor deposition of TCNQ gas on a metallic Cu^0 surface,[8−11] solution reaction of TCNQ with Cu^0 metal in organic solvents,[5,12] and chemical/electrochemical/photochemical reduction of TCNQ in the presence of Cu^+ or Cu^{2+} ions.[6,13,14] However, the chemical vapor techniques required an inert atmosphere since Cu^0 was quickly oxidized when directly exposed to air,[15] and also a high temperature (over 100 °C) was needed.[8] Although the other methods made progress in the fabrication of micro- and nanoscale Cu–TCNQ structures, the controlled growth of this nanoscale crystal with reproducible uniform morphology in less harsh environment at room temperature is still challenging. To solve this problem, microfluidic technology was shown to be an optimal approach, due to its possibility of precise fluid handling, allowing spatially controllable reactions.[16−19]

Received: February 3, 2017
Accepted: April 26, 2017
Published: April 26, 2017

DOI: 10.1021/acsami.7b01664
ACS Appl. Mater. Interfaces 2017, 9, 17271−17278

In addition, reported studies on the switching effect of Cu−TCNQ showed that the traditional sandwich electrode structures with aluminum (Al) could influence the conductive behavior of this organic material.[20,21] Thus, the use of nonsandwich devices and metals other than Al as electrodes is highly desired in studying the conductive behavior of Cu−TCNQ.[7,22]

In this work, a microchamber array developed by our group[23] was adopted and greatly improved for the localized formation of Cu−TCNQ nano/microscale structures in ultrasmall microchambers. This method allows not only continuous and multiple chemical reactions in confined microchambers but also excellent fluid handling which ensures the reaction of TCNQ with a trapped Cu^0 layer. This is also the first on-chip conversion of Cu^0 into Cu−TCNQ nanostructures. Furthermore, since the synthesis is carried out in a solution phase inside the microchip, efficient reduction of exogenous oxygen into the system is possible when pretreated (argon gas flushed) solutions are used. With the proposed method, the morphology of Cu−TCNQ nano/microstructures was controlled by adjusting the concentration of precursors and the reaction time. Outcomes of this method were analyzed by scanning electron microscopy (SEM). Moreover, the conductive property and reversible switching effect of such synthesized Cu−TCNQ nanostructures were tested by using integrated Pt microelectrode arrays to avoid the effects from the electrode system. In combination with integrated electrodes in the microchambers, a direct bottom contact of Cu−TCNQ with Pt microelectrodes is achievable without further complicated manipulations. This work represents the first attempt to synthesize Cu−TCNQ nanostructures by microfluidic-assisted techniques in a "normal" environment at room temperature, with direct integration into an electrode system for conductive measurement.

2. EXPERIMENTAL SECTION

2.1. Materials. Positive photoresist AZ-9260 and AZ-400 K developers were purchased from Microchemicals (Ulm, Germany). 1*H*,1*H*,2*H*,2*H*-Perfluorodecyl-dimethylchlorosilane was purchased from ABCR (Karlsruhe, Germany), and poly(dimethylsiloxane) (PDMS) (Sylgard 184) was obtained from Dow Corning (Midland, MI, USA). Acetonitrile (CH_3CN, 99.8+%), copper(II) sulfate ($CuSO_4$, anhydrous, powder, ≥99.99% trace metals basis), ethanol (CH_3CH_2OH, 99.8+%), sodium borohydride ($NaBH_4$, powder, ≥98.0%), sodium citrate dehydrate ($C_6H_5O_7Na_3{\cdot}2H_2O$), sodium hydroxide (NaOH, reagent grade, ≥98%, pellets) were all purchased from Sigma-Aldrich (Buchs, Switzerland). 7,7,8,8-Tetracyanoquinodimethane (TCNQ, >98.0%, HPLC) was obtained from TCI (Eschborn, Germany). Ultrapure deionized (DI) water (Mill-Q purifiers, 18.2 MΩ·cm at 25 °C) was used throughout the experiment.

2.2. Chip Design and Fabrication of the Double-Layer Microchips. The microfluidic chip used here was an improved chip design based on the microchamber array designed before,[23] but here with further reduced volumes. Generally, a 50 μm wide microchamber design was used, with modified fluid inlet and outlet designs and gas control channels. A four-electrode system with eight pairs of electrodes was integrated into the microchip for a four-point measurement. Each pair of electrodes was aligned to a microchamber separately. Detailed methods for master mold fabrication, multilayer chip assembly, and patterning of microelectrodes also refer to the reported work.[23] Finally, in order to avoid introducing air into the microchip when solutions were changed, two reservoirs were added onto the two inlets after the assembly of the multilayer chip.

2.3. Microchip Operation. Control layer channels were filled with water by centrifugation before the experiments. Custom-made metal connectors and silicone tubing were used to introduce N_2 gas into the control layer of the microchip. The gas channel in the control layer was pressurized up to 3 bar for closing the microchambers and stopping fluid flows. It was released to 2 bar to allow the slow diffusion of solutions into the microchambers. In the fluid layer, the reagents were loaded into plastic syringes and supplied through Teflon tubing into the microchip using a software controlled syringe-pump system (neMESYS module, Cetoni GmbH Korbußen, Germany).

2.4. *In Situ* Formation of Cu−TCNQ Nano/Microstructures. *Solution Preparation.* $CuSO_4$ and $C_6H_5O_7Na_3{\cdot}2H_2O$ powders were dissolved in DI water separately to form solutions of concentrations up to 0.5 M. A 1 M $NaBH_4$ solution was prepared by using NaOH solution (pH = 12) as the solvent. A high pH value was used to stabilize $NaBH_4$. TCNQ was dissolved in CH_3CN at concentrations of 2 and 5 mM, respectively. Other concentrations of solutions were obtained by diluting the above-mentioned solutions using their separate solvents. In addition, to avoid air in the experiment, all the solutions were flushed using Ar gas for 20 min before use.

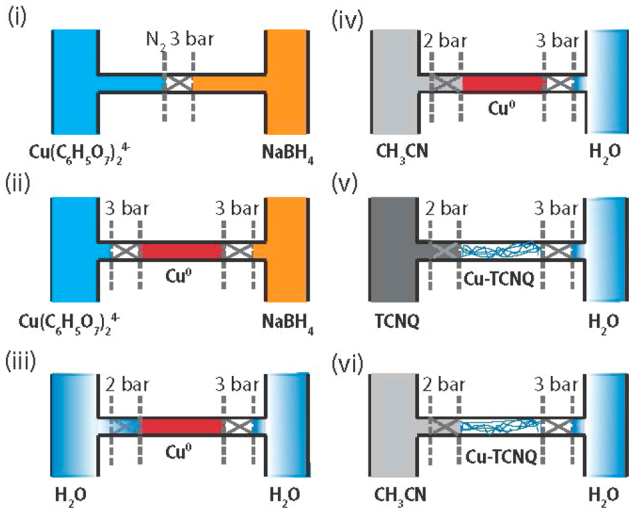

Figure 1. Schematic illustration of the formation of Cu−TCNQ nano/microstructures in solution inside a subnanoliter microchamber. Solid lines show one microchamber, and dashed lines indicate the pressurized gas channels. See section 2.4 for details.

Synthesis of Cu^0 Layer and Cu−TCNQ. As illustrated in Figure 1, the formation of Cu^0 and Cu−TCNQ was achieved by the following steps:

(i) The middle control channel was pressed to 3 bar by N_2 gas to close the middle of the chamber. $Cu(C_6H_5O_7)_2^{4-}$ (obtained after mixing $CuSO_4$ and $C_6H_5O_7Na_3$, see section 3.2) and $NaBH_4$ solutions were supplied from two inlets (Figure 1, (i)).

(ii) The two side gas channels were pressurized to 3 bar to stop supplying solutions. Then the middle gas channel was released to allow the two solutions to mix. This led to the formation of Cu^0 (Figure 1, (ii)).

(iii) DI water was supplied from the inlets. The left gas channel was released to 2 bar to allow water to slowly diffuse into the chamber and wash Cu^0 (Figure 1, (iii)).

(iv) CH_3CN was supplied (instead of water) from the left inlet to diffuse into the chamber and wash Cu^0 (Figure 1, (iv)).

(v) TCNQ solution was supplied (instead of water) to diffuse into the microchamber and react with Cu^0. Different morphologies of the structures were observed after the reaction (Figure 1, (v)).

(vi) The solvent, CH_3CN, was introduced to wash off the TCNQ solution in the channel and microchambers (Figure 1, (vi)).

DOI: 10.1021/acsami.7b01664
ACS Appl. Mater. Interfaces 2017, 9, 17271−17278

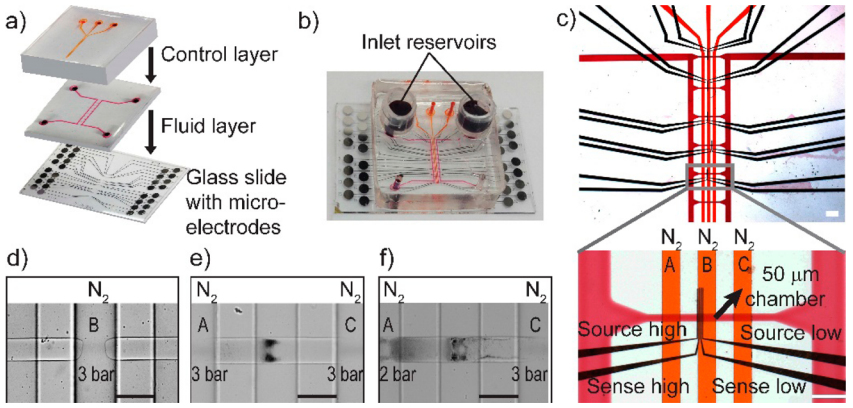

Figure 2. Microchip device for the synthesis of Cu−TCNQ structures. (a) Schematic of the alignment of the microchip. (b) Photograph of the final device with two reservoirs added to the inlets after the alignment of the microchip. The glass slide is 24 mm × 40 mm in size, and the dimensions of the microchip are 24 mm × 24 mm × 6 mm. (c) Top: optical image of the microchip, with orange and red food dyes in the control and fluidic layers, respectively. Bottom: magnification of one reaction microchamber (50 μm in width) with aligned microelectrodes. The four electrodes used in this experiment are shown in this image, with source high and source low electrodes outside and sense high and sense low electrodes inside. Scale bars: 200 μm. (d)−(f) Operation of gas channels with (d) the middle gas channel B is pressurized to 3 bar to close the chamber, (e) the two side gas channels A and C are pressurized to 3 bar to stop flows and allow the reaction inside the microchamber (black products started to form from the middle indicating the formation of Cu^0), and (f) the channel A was released to 2 bar to allow the slow solvent exchange in the microchamber and to wash the Cu^0 formed inside the chamber. Scale bars: 100 μm.

Finally, the microchip was put in a vacuum to allow for evaporation of the solvent. The resulting nano/microstructures were obtained in the microchambers.

2.5. Characterization. Colored images were recorded on a stereomicroscope (AZ-100M, Nikon) equipped with a digital camera (Digital sight DS-Fi1, Nikon). Other optical images were taken on an inverted microscope (IX71, Olympus) equipped with a digital camera (UK1117, ABS) and standard filters. Absorption spectra were obtained on a UV−vis spectrophotometer (V-650, JASCO). The IR transmission measurements were performed using a TENSOR 37 (Bruker) FT-IR spectrometer. The spectral resolution was set to 4 cm^{-1}. Raman spectra were obtained on a confocal Raman microscope (NanoScan Technology) equipped with a diode-pumped solid-state (DPSS) laser (Cobolt Samba, λ = 532 nm) and a 50× Olympus objective (NA 0.75). The laser power was 0.4 mW, and the accumulation time was 60 s. The SEM images and the energy dispersive X-ray spectroscopy (EDX-SEM) were obtained using a FEI Quanta 200 FEG at the Scientific Centre for Optical and Electron Microscopy (ScopeM) of ETH Zürich.

To measure the electrical properties of the nanostructures, the microchip was dried in vacuum after the synthesis. Afterward, four Pt microelectrodes (5 μm gap) which enabled top contact with *in situ* formed nanostructures in a confined microchamber were used for a four-point measurement, with a signal reading from Au needle probes in contact with Pt microelectrodes (Figure S1, Supporting Information). For *I*−*V* curve measurements, current was applied through the outer electrode pair (source high and source low) and the resulting potential on the inner electrode pair (sense high and sense low) was monitored using a Keithley 2612A system source meter.[24] For testing the electrical switching effect, a voltage sweep was used.

2.6. Data Processing. Raman spectra were recorded using NSpec software (NanoScan Technology, GmbH). IR spectra were recorded by the OPUS software (21 CFR Part 11 compliant). The Raman and IR spectra of TCNQ and Cu−TCNQ were analyzed with Origin Pro 9.1 (Academic) (Originlab Corporation). Conductivity results were recorded by the TSP Express Software Tool and analyzed with Origin Pro 9.1 (Academic) (Originlab Corporation).

3. RESULTS AND DISCUSSION

3.1. Microchip with Chamber Array. As shown in Figure 2a, the microfluidic device was a double-layer microchip made of PDMS by soft lithography,[25,26] with a top control layer consisting of three gas channels and a fluid layer with ten parallel microchambers, separated by a thin and flexible PDMS membrane. The multilayer chip was assembled and integrated to a glass slide with prepatterned microelectrodes to form the final device (Figure 2a,b). The mirochambers were operated by the three parallel control channels upon pressurization with N_2 gas (see section 2.4 for details). Compared to the microchamber array for Ag−TCNQ reported by our group,[23] several aspects were improved in this new chip design. First, 50 μm wide microchambers were fabricated to reduce the volume of solutions required to a subnanoliter volume. Second, the microchannel toward inlet and outlet of the fluid layer were changed in order to better control the fluids into the ultrasmall chambers. Third, for the electrical measurement of the structures formed in microchambers, a four-electrode system (source high, source low, sense high, and sense low) was used in the four-point probe measurement (Figure 2c), instead of the two-point method.[23] These improvements helped to precisely control the growth conditions of Cu−TCNQ and made a detailed in situ analysis possible. The synthesis of Cu^0 in the microchamber by controlling the gas channels is shown in Figure 2d−f (detailed experimental procedure see section 2.4).

3.2. Reaction Mechanism (Scheme S1, Supporting Information). Cu−TCNQ structures were synthesized by using Cu^0 and TCNQ solution in CH_3CN. Cu^0 was produced from an electroless Cu-plating solution consisting of a copper salt ($CuSO_4$), a complexing agent ($C_6H_5O_7Na_3$), a reducing agent ($NaBH_4$), and NaOH to adjust the pH. Here, $C_6H_5O_7Na_3$ is used as an organic chelating agent that interacts with $CuSO_4$ and solubilizes Cu^{2+} ions present in solution, to form a Cu−chelator complex.[15]

3.3. Controlled Synthesis of Cu^0 and Cu−TCNQ Nano/Microstructures on Microchips. Since Cu^0 can easily be oxidized when in contact with air,[27] special precautions were taken to efficiently reduce oxygen in the microchips. First of all, all the solutions were flushed with Ar gas for 20 min before the experiment. Then, two reservoirs were filled with water or CH_3CN (Figure 2b), with the purpose of avoiding air bubbles being introduced into the microchannels during the experiment. With this microchip, the localized synthesis of Cu^0 inside

DOI: 10.1021/acsami.7b01664
ACS Appl. Mater. Interfaces 2017, 9, 17271−17278

Table 1. Morphology of Structures Formed under Different Reaction Conditions on Microchips

$[Cu(C_6H_5O_7)_2^{4-}]/[NaBH_4]$ (mM)	[TCNQ] (mM)	reaction time (min)	morphology of products[a] (Φ diameter, μm; L length, μm)
250/500	5	10	short nano/microrods (0.4−1), (5−10)
50/100	5	10	long nano/microrods (0.8−1.5), (10−50)
25/50	2	10	nanowire bundles (0.1−0.8), (5−20)
25/50	2	20	microrods

[a]The optical and SEM images are shown in Figure S1 and Figure 4a,b.

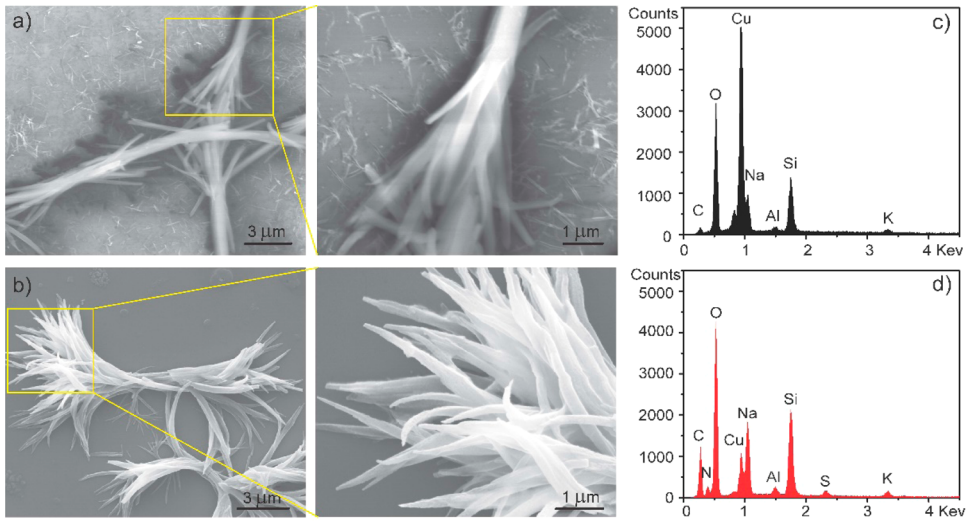

Figure 3. (a) and (b) SEM images of Cu−TCNQ nanowire bundles (100−800 nm in diameter, 5−20 μm in length), with the magnification of wire bundles marked with the yellow box. The EDX spectrum of the (c) Cu^0 layer (notice the strong Cu element signal) and the (d) Cu−TCNQ nanowire bundles. Notice the appearance of the N element, the obvious increase in C, and the decrease in Cu signals, compared to that of Cu (Figure 3c). The strong O signals in the EDX spectra were mainly obtained from a glass slide (Figure S4a, Supporting Information) and presumably from the oxidation of samples upon exposure to air.

the microchamber was achieved by adjusting the pressure into the gas channels to 3 bar (Figure 2d,e). Finally, after the formation and washing of Cu^0, the direct synthesis of the charge-transfer compound Cu−TCNQ was achieved by slightly opening the valves to allow the diffusion of TCNQ solutions into confined microchambers with trapped Cu^0 particles (Figure 2f and Figure 1v).

The Cu^0 formed via this method appeared brown in color and shiny as a metal, as observed by eye on a glass slide of a nonbonded chip (Figure S2a, Supporting Information), as well as under an optical microscope on a glass slide (Figure S2c, Supporting Information) and in a microchannel (Figure S2d,e, Supporting Information). After the reaction of Cu with TCNQ solutions on a nonbonded chip, a dark blue product was obtained on the glass slide (Figure S2b, Supporting Information), indicating the formation of Cu−TCNQ.[28] The wire morphology inside a microchamber was observed under a microscope (Figure S2f, Supporting Information). With the microfluidic techniques, the density of the Cu^0 layer and the morphologies of Cu−TCNQ were formed in a controlled way, for example, by using different concentrations of precursors and controlling the reaction time (Table 1).

High concentrations of $Cu(C_6H_5O_7)_2^{4-}/NaBH_4$ (250/500 mM) resulted in a thick Cu^0 layer (Figure S3a, Supporting Information). Upon reaction with 5 mM TCNQ at a flow rate of 2 μL/min for 10 min, dense short nano/microrods (0.4−1 μm in diameter, 5−10 μm in length) were observed (Figure S3b,c, Supporting Information). However, 5 times diluted $Cu(C_6H_5O_7)_2^{4-}/NaBH_4$ solutions (50/100 mM) resulted in large particles of Cu^0 (Figure S3d, Supporting Information), followed by the formation of long nano/microrods after reacting with 5 mM TCNQ for 10 min (Figure S3e,f, Supporting Information) (structures with 0.8−1.5 μm in diameter, 10−50 μm in length). In contrast, a very low concentration of the $Cu(C_6H_5O_7)_2^{4-}/NaBH_4$ solution (25/50 mM) was used and led to the formation of a thin Cu^0 layer in the channel (Figure S3g, Supporting Information), after reacting with a low concentrated TCNQ solution (2 mM) for 10 min. In this case, bundles of nanowire structures were observed (Figure S3h, Supporting Information), as also seen by SEM results (Figure 3a,b). In addition, a longer reaction time (20 min) caused the formation of larger structures (Figure S3i, Supporting Information), compared to those in Figure S3h (Supporting Information). This may be due to the aggregation of wire structures.[5] Using high concentrations of $Cu(C_6H_5O_7)_2^{4-}/NaBH_4$ (250/500 mM), bubbles were observed in the channel, likely due to the release of hydrogen in the redox reaction between $NaBH_4$ and water (eq 2 in Scheme S1, Supporting Information).[15,29−31] Instead, this was not observed when low concentrated solutions were used. Thus, a low concentration of precursors ($Cu(C_6H_5O_7)_2^{4-}/NaBH_4$, 25/50 mM) and a short reaction time (10 min) are ideal for the synthesis of nanometer scaled Cu−TCNQ structures.

3.4. Characterization of Cu−TCNQ Nano/Microstructures. Detailed characterization was performed to confirm the composition and properties of the as-prepared nano/microstructures. As shown in Figure 3, the compositions of Cu^0 and resulted Cu−TCNQ were determined by the EDX-SEM spectra (Figure 3c,d).

DOI: 10.1021/acsami.7b01664
ACS Appl. Mater. Interfaces 2017, 9, 17271−17278

In addition, the UV−vis spectra of neutral TCNQ and Cu−TCNQ solutions were obtained, with the latter from the eluted solution of a nonbonded microchip after synthesis. As indicated in Figure 4a, neutral TCNQ showed only one peak at 393 nm.

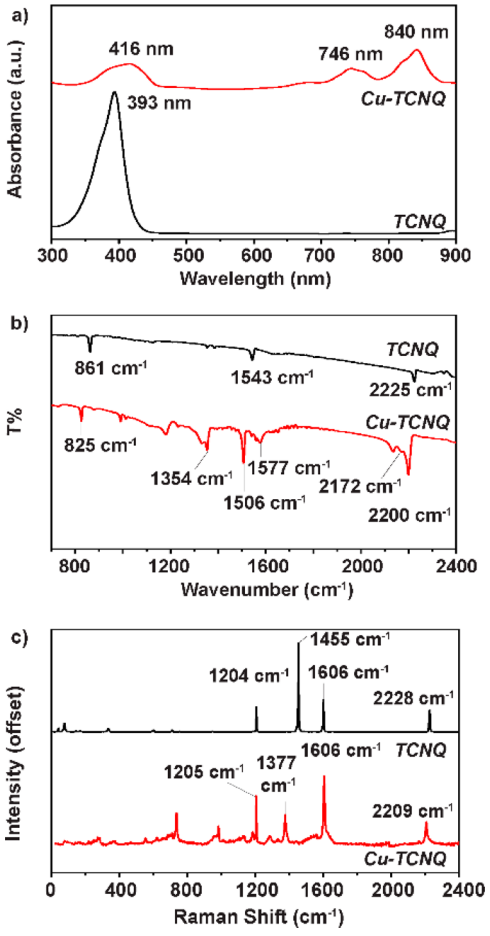

Figure 4. (a) UV−vis absorption spectra of TCNQ (black) and Cu−TCNQ (red) solutions in CH_3CN. (b) FT-IR and c) Raman spectra of TCNQ and Cu−TCNQ nanowires obtained from nonbonded microchips at the concentration of $Cu(C_6H_5O_7)_2^{4-}$/$NaBH_4$ (25/50 mM) after reacting with 2 mM TCNQ.

In contrast, the Cu−TCNQ solution exhibited a broad peak at 416 nm and exhibited absorption peaks at 746 and 840 nm, which could be assigned to TCNQ anion radicals in the sample.[5] FT-IR and Raman measurements were carried out in order to determine the oxidation state of TCNQ molecules in neutral TCNQ and Cu−TCNQ nanostructures. As can be seen from the IR spectra (Figure 4b), compared to the spectrum of pure TCNQ, the C═C—H mode of Cu−TCNQ shifted from 861 to 825 cm^{-1}. In addition, the C═C ring stretching peak at 1543 cm^{-1} split into two peaks at 1506 and 1577 cm^{-1}. Typically, the peak at 1506 cm^{-1} denoted the formation of TCNQ anion radicals.[5] The C═C wing-stretching region was also represented by the peak at 1354 cm^{-1}. Moreover, the strong band at ~2200 cm^{-1} was associated with the C≡N stretching mode. Apart from these, the Raman spectral analysis of Cu−TCNQ (Figure 4c) showed the main characteristic vibration modes at 1205 cm^{-1} (C═C—H bending), 1377 cm^{-1} (C—CN stretching), 1606 cm^{-1} (C═C ring stretching), and 2209 cm^{-1} (C≡N stretching). Compared to the Raman spectrum of a neutral TCNQ crystal, the C—CN stretching mode in Cu−TCNQ shifted from 1455 to 1377 cm^{-1} because of the complete charge transfer between Cu^0 and TCNQ molecules.[8,32] Thus, the FT-IR and Raman spectra results clearly proved the composition of Cu−TCNQ in these nanostructures.

The larger microstructures formed at higher concentrations of precursors (Figure S3e,f, Supporting Information) were also characterized by EDX-SEM (Figure S4, Supporting Information), FT-IR, and Raman spectroscopy (Figure S5, Supporting Information). These spectra showed that the microstructures exhibited similar charateristics to the nanostructures, suggesting a similar composition of these structures.

3.5. Conductive Measurement of Cu−TCNQ Nanostructrues. To test the possibility of a direct integration onto microelectrodes and to characterize the electrical properties of Cu−TCNQ nanostructures, the *I*−*V* curves of the Cu^0 layer before and after reacting with TCNQ solutions were obtained on-chip by four-point probe measurements after solvent evaporation in a vacuum. The graph in Figure 5a shows a linear *I*−*V* sweep for the copper layer, indicating its typical metallic nature. In contrast, after the formation of nanostructures (100−800 nm in diameter, 5−20 μm in length) inside different microchambers, nonlinear *I*−*V* curves were obtained (Figure 5b). The quasi-symmetric character of the *I*−*V* curves for wire bundles indicates the formation of Cu−TCNQ crystals and the good contact with the prefabricated microelectrodes inside the microchamber. Reproducible *I*−*V* responses indicate the possible application of this technique for parallelized integration of conductive nanowires. Moreover, the electrical properties of the synthesized nanowire devices were proven to be stable in air. The conductive behavior of larger microstructures was also tested (Figure S6, Supporting Information), and the nonlinearity of their *I*−*V* curve clearly proved the conductive behavior of Cu−TCNQ microwire structures.

When a reversible voltage from 0 to 10 V was applied to the nanowire bundles, reversible hysteretic *I*−*V* curves were observed (Figure 5c). In addition, the two switchable states were confirmed and attributed to high and low impedance, respectively. The reversible hysteretic *I*−*V* curves proved the good switching behavior of the Cu−TCNQ nanowire bundles, which also confirmed the importance of this organic memory material in the switching process.[10] In addition, we tested the oxygen persistence of Cu−TCNQ nanostructures by measuring the conductivity on the same nanostructure device before and after air exposure at different times (Figure S7). The *I*−*V* curves show that the conductivity decreases slowly over 72 h to a constant value, which indicates an oxidation process; however, difficulties in the contact between electrodes and structures may have contributed to this decrease as well.

There was evidence in former studies that the switching mechanism of the Cu−TCNQ film involved a composition change.[33] The composition of the switching states consists of $M^+TCNQ^{-\bullet}$ that shows high electrical resistivity and $M^+(TCNQ^{-\bullet})TCNQ$, with neutral TCNQ in the structure, that exhibits low electrical resistivity (Scheme 1).

However, there is still inconsistency in reported studies concerning the switching effect of Cu−TCNQ. Some researchers suggested that the switching behavior was associated with phase changes in bulk samples (from phase II to phase I) after application of the electric field,[13] while others proposed that this effect was caused by the contact of the Al electrode with the Cu−TCNQ surface.[20,21] In our study, a device with Pt electrode systems was applied. We observed the

DOI: 10.1021/acsami.7b01664
ACS Appl. Mater. Interfaces 2017, 9, 17271−17278

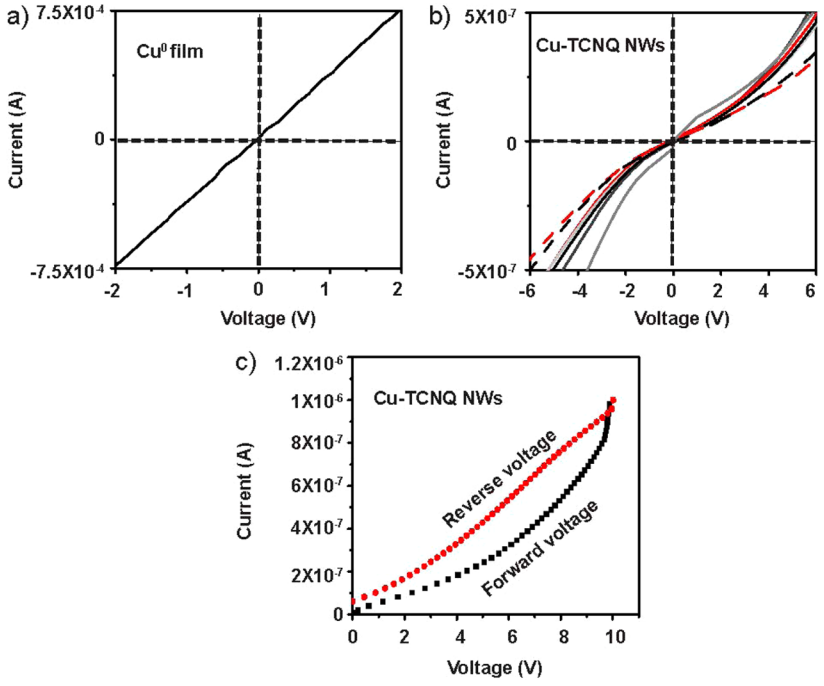

Figure 5. Typical room-temperature $I-V$ characteristics of the (a) Cu^0 layer and (b) multiple $I-V$ sweeps of different integrated Cu−TCNQ nanowire bundles in different microchambers. (c) $I-V$ curves recorded for Cu−TCNQ nanowire (NW) bundles showing hysteresis in the electrical response after sweeping the applied reversible voltage from 0 to 10 V, with the forward voltage curve and reverse voltage curve correlating to "high impedance" and "low impedance" states, respectively.

Scheme 1. "High Impedance" and "Low Impedance" Reversible Switching States of Cu−TCNQ Complexes upon Voltage Sweeping[a]

$$\underset{\text{High-impedance}}{\left[Cu^{+}TCNQ^{-}\right]_{n}} \overset{\text{voltage}}{\rightleftharpoons} Cu_x^{0} + TCNQ^{0}{}_x + \underset{\text{Low-impedance}}{\left[Cu^{+}TCNQ^{-}\right]_{n-x}}$$

[a]Upon the reaction with electron donors, the strong π-acid TCNQ can undergo complete electron transfer to form the anion radical $TCNQ^{-\bullet}$. The resulting complexes have two series of crystalline structures, with the first series of $Cu^{+}TCNQ^{-\bullet}$, showing high electrical resistivity ("high impedance"), and the second one of $Cu^{+}(TCNQ^{-\bullet})$-TCNQ, involving neutral TCNQ in the structure and exhibiting low electrical resistivity ("low impedance") ($0 < x \leq n$).

electric-field-induced reversible hysteretic switching effect of our nanowire bundles, in accordance with the observations of Müller et al.[10] and Xiao et al.,[8,34] though the detailed working mechanism is yet to be understood.

4. CONCLUSIONS

In conclusion, the microfluidic-based synthesis of conductive Cu−TCNQ in an ambient environment at room temperature was achieved. Different morphologies of Cu−TCNQ nano/microstructures could be synthesized in a controlled way by tuning the concentration of precursors and by changing the reaction time inside microchips. With this technique, reactions were confined in parallel ultrasmall microchambers. Thus, the nanostructures were locally formed and integrated with prefabricated microelectrodes, and moreover, their electrical properties could be measured directly, without further micromanipulation. Cu−TCNQ nanostructures formed with the proposed method showed a conductive behavior and a reversible hysteretic switching effect upon an electric field, indicating the possibility of using this technique for the building of nanoelectronics and nanoswitches in an easy and efficient way. Although inconsistent switching mechanisms of Cu−TCNQ were reported in former studies, our observations correlate well with some previous findings.[8,10,34] For clarification, a detailed study of the switching mechanism has to be done. Work along this way is under investigation in our laboratory.

■ ASSOCIATED CONTENT

Supporting Information

The Supporting Information is available free of charge on the ACS Publications website at DOI: 10.1021/acsami.7b01664.

Schematic 3D view of a microchamber, the scheme of reaction mechanism, optical images of Cu^0 and Cu−TCNQ nano/microstructures, characterization (EDX-SEM, FT-IR, Raman), $I-V$ curve of Cu−TCNQ microstructures and changes in conductivity of Cu−TCNQ nanowires upon air exposure (PDF)

■ AUTHOR INFORMATION

Corresponding Author

*Tel: (+)41 61 387 33 10. E-mail: petra.dittrich@bsse.ethz.ch. (P. Dittrich)

ORCID

Petra S. Dittrich: 0000-0001-5359-8403

Author Contributions

The manuscript was written through contributions of all authors. All authors have given approval to the final version of the manuscript.

Funding

We acknowledge funding from the Excellence Initiative Deutsche Forschungsgemeinschaft (DFG). Financial support from the "Senatsverwaltung für Wirtschaft, Technologie und

DOI: 10.1021/acsami.7b01664
ACS Appl. Mater. Interfaces 2017, 9, 17271−17278

Forschung des Landes Berlin", the "Ministerium für Innovation, Wissenschaft und Forschung des Landes Nordrhein-Westfalen", and the "Bundesministerium für Bildung und Forschung" is also acknowledged.

Notes

The authors declare no competing financial interest.

■ ACKNOWLEDGMENTS

We thank the Scientific Center for Optical and Electron Microscopy (ScopeM) of ETH Zürich for their facilities. We thank M. Lenz for the chip design and Y. Schmid for the fabrication of glass slides with microelectrodes. We also thank Z. Zhang from the SALSA graduate school for the UV−vis measurements and Maria Becker from ISAS Dortmund for the SEM measurements.

■ REFERENCES

(1) Inoue, M. B.; Inoue, M.; Fernando, Q.; Nebesny, K. W. Tetracyanoquinodimethan Salts of Copper Chelate with Tetrabenzo-[b,f,j,n][1,5,9,13]tetraazacyclohexadecine: Electrical Properties and Mixed-Valence States. *J. Phys. Chem.* **1987**, *91* (3), 527−530.

(2) Potember, R. S.; Hoffman, R. C.; Hu, H. S.; Cocchiaro, J. E.; Viands, C. A.; Poehler, T. O. Electronic Devices from Conducting Organics and Polymers. *Polym. J.* **1987**, *19* (1), 147−156.

(3) Kaim, W.; Moscherosch, M. The Coordination Chemistry of TCNE, TCNQ and Related Polynitrile π Acceptors. *Coord. Chem. Rev.* **1994**, *129* (1), 157−193.

(4) Azcondo, M. T.; Ballester, L.; Golhen, S.; Gutierrez, A.; Ouahab, L.; Yartsev, S.; Delhaes, P. Structural, Magnetic, Electrical and Optical Characterization of Systems Built from $[M([9]aneN_3)_2]^{2+}$ (M = Cu^{II} or Ni^{II}) and TCNQ or $TCNQF_4$. *J. Mater. Chem.* **1999**, *9* (6), 1237−1244.

(5) Liu, Y.; Ji, Z.; Tang, Q.; Jiang, L.; Li, H.; He, M.; Hu, W.; Zhang, D.; Jiang, L.; Wang, X.; Wang, C.; Liu, Y.; Zhu, D. Particle-Size Control and Patterning of a Charge-Transfer Complex for Nanoelectronics. *Adv. Mater.* **2005**, *17* (24), 2953−2957.

(6) O'Mullane, A. P.; Fay, N.; Nafady, A.; Bond, A. M. Preparation of Metal−TCNQ Charge-Transfer Complexes on Conducting and Insulating Surfaces by Photocrystallization. *J. Am. Chem. Soc.* **2007**, *129* (7), 2066−2073.

(7) He, L. F.; Ji, Z. Y.; Zhen, Y. G.; Liu, J.; Yang, F. X.; Zhao, Q.; Dong, H. L.; Hu, W. P. Single-Displacement Controlled Spontaneous Electrolysis towards CuTCNQ Microribbon Electrodes in Organic Single-Crystal Transistors. *Phys. Chem. Chem. Phys.* **2015**, *17* (40), 26541−26544.

(8) Xiao, K.; Ivanov, I. N.; Puretzky, A. A.; Liu, Z.; Geohegan, D. B. Directed Integration of Tetracyanoquinodimethane-Cu Organic Nanowires into Prefabricated Device Architectures. *Adv. Mater.* **2006**, *18* (16), 2184−2188.

(9) Zheng, K. B.; Shen, H. T.; Ye, C. N.; Li, J. L.; Sun, D. L.; Chen, G. R. The Electrical Switching Characteristics of Single Copper Tetracyanoquinodimethane Nanowire. *Nano-Micro Lett.* **2009**, *1* (1), 23−26.

(10) Müller, R.; De Jonge, S.; Myny, K.; Wouters, D. J.; Genoe, J.; Heremans, P. Organic CuTCNQ Integrated in Complementary Metal Oxide Semiconductor Copper Back End-of-line for Nonvolatile Memories. *Appl. Phys. Lett.* **2006**, *89* (22), 223501.

(11) Liu, Y. L.; Li, H. X.; Tu, D. Y.; Ji, Z. Y.; Wang, C. S.; Tang, Q. X.; Liu, M.; Hu, W. P.; Liu, Y. Q.; Zhu, D. B. Controlling the Growth of Single Crystalline Nanoribbons of Copper Tetracyanoquinodimethane for the Fabrication of Devices and Device Arrays. *J. Am. Chem. Soc.* **2006**, *128* (39), 12917−12922.

(12) Ji, H.-X.; Hu, J.-S.; Guo, Y.-G.; Song, W.-G.; Wan, L.-J. Ion-Transfer-Based Growth: A Mechanism for CuTCNQ Nanowire Formation. *Adv. Mater.* **2008**, *20* (24), 4879−4882.

(13) Heintz, R. A.; Zhao, H.; Ouyang, X.; Grandinetti, G.; Cowen, J.; Dunbar, K. R. New Insight into the Nature of Cu(TCNQ): Solution Routes to Two Distinct Polymorphs and Their Relationship To Crystalline Films That Display Bistable Switching Behavior. *Inorg. Chem.* **1999**, *38* (1), 144−156.

(14) Neufeld, A. K.; O'Mullane, A. P.; Bond, A. M. Control of Localized Nanorod Formation and Patterns of Semiconducting CuTCNQ Phase I Crystals by Scanning Electrochemical Microscopy. *J. Am. Chem. Soc.* **2005**, *127* (40), 13846−13853.

(15) Li, D.; Sutton, D.; Burgess, A.; Graham, D.; Calvert, P. D. Conductive Copper and Nickel Lines via Reactive Inkjet Printing. *J. Mater. Chem.* **2009**, *19* (22), 3719−3724.

(16) Paquet, C.; Jakubek, Z. J.; Simard, B. Superparamagnetic Microspheres with Controlled Macroporosity Generated in Microfluidic Devices. *ACS Appl. Mater. Interfaces* **2012**, *4* (9), 4934−4941.

(17) Cheng, Y.; Yu, Y.; Fu, F.; Wang, J.; Shang, L.; Gu, Z.; Zhao, Y. Controlled Fabrication of Bioactive Microfibers for Creating Tissue Constructs Using Microfluidic Techniques. *ACS Appl. Mater. Interfaces* **2016**, *8* (2), 1080−1086.

(18) Dendukuri, D.; Pregibon, D. C.; Collins, J.; Hatton, T. A.; Doyle, P. S. Continuous-Flow Lithography for High-throughput Microparticle Synthesis. *Nat. Mater.* **2006**, *5* (5), 365−369.

(19) Hansen, C. L.; Skordalakes, E.; Berger, J. M.; Quake, S. R. A Robust and Scalable Microfluidic Metering Method that Allows Protein Crystal Growth by Free Interface Diffusion. *Proc. Natl. Acad. Sci. U. S. A.* **2002**, *99* (26), 16531−16536.

(20) Sato, C.; Wakamatsu, S.; Tadokoro, K.; Ishii, K. Polarized Memory Effect in the Device Including the Organic Charge-Transfer Complex, Copper-Tetracyanoquinodimethane. *J. Appl. Phys.* **1990**, *68* (12), 6535−6537.

(21) Hoagland, J. J.; Wang, X. D.; Hipps, K. W. Characterization of Cu-CuTCNQ-M Devices Using Scanning Electron Microscopy and Scanning Tunneling Microscopy. *Chem. Mater.* **1993**, *5* (1), 54−60.

(22) Liu, Y. L.; He, M.; Meng, Q.; Tang, Z. Y.; Li, L. Q.; Hu, W. P. Mass-Production of Single-Crystalline Device Arrays of an Organic Charge-Transfer Complex for its Memory Nature. *Small* **2012**, *8* (4), 557−560.

(23) Cvetković, B. Z.; Puigmartí-Luis, J.; Schaffhauser, D.; Ryll, T.; Schmid, S.; Dittrich, P. S. Confined Synthesis and Integration of Functional Materials in Sub-nanoliter Volumes. *ACS Nano* **2013**, *7* (1), 183−190.

(24) Xing, Y.; Esser, N.; Dittrich, P. S. Conductive Single Nanowires Formed and Analysed on Microfluidic Devices. *J. Mater. Chem. C* **2016**, *4* (39), 9235−9244.

(25) Unger, M. A.; Chou, H.-P.; Thorsen, T.; Scherer, A.; Quake, S. R. Monolithic Microfabricated Valves and Pumps by Multilayer Soft Lithography. *Science* **2000**, *288* (5463), 113−116.

(26) Küchler, A.; Bleich, J. N.; Sebastian, B.; Dittrich, P. S.; Walde, P. Stable and Simple Immobilization of Proteinase K Inside Glass Tubes and Microfluidic Channels. *ACS Appl. Mater. Interfaces* **2015**, *7* (46), 25970−25980.

(27) Kim, J. H.; Ehrman, S. H.; Germer, T. A. Influence of Particle Oxide Coating on Light Scattering by Submicron Metal Particles on Silicon Wafers. *Appl. Phys. Lett.* **2004**, *84* (8), 1278−1280.

(28) Liu, H. B.; Li, J. B.; Lao, C. S.; Huang, C. S.; Li, Y. L.; Wang, Z. L.; Zhu, D. B. Morphological Tuning and Conductivity of Organic Conductor Nanowires. *Nanotechnology* **2007**, *18* (49), 495704.

(29) Glavee, G. N.; Klabunde, K. J.; Sorensen, C. M.; Hadjipanayis, G. C. Borohydride Reduction of Nickel and Copper Ions in Aqueous and Nonaqueous Media. Controllable Chemistry Leading to Nanoscale Metal and Metal Boride Particles. *Langmuir* **1994**, *10* (12), 4726−4730.

(30) Kojima, Y.; Suzuki, K.-i.; Fukumoto, K.; Sasaki, M.; Yamamoto, T.; Kawai, Y.; Hayashi, H. Hydrogen Generation Using Sodium Borohydride Solution and Metal Catalyst Coated on Metal Oxide. *Int. J. Hydrogen Energy* **2002**, *27* (10), 1029−1034.

(31) Muir, S. S.; Yao, X. Progress in Sodium Borohydride as a Hydrogen Storage Material: Development of Hydrolysis Catalysts and Reaction Systems. *Int. J. Hydrogen Energy* **2011**, *36* (10), 5983−5997.

(32) Gucciardi, P. G.; Trusso, S.; Vasi, C.; Patane, S.; Allegrini, M. Nano-Raman Imaging of Cu-TCNQ Clusters in TCNQ Thin Films by

DOI: 10.1021/acsami.7b01664
ACS Appl. Mater. Interfaces 2017, 9, 17271−17278

Scanning Near-Field Optical Microscopy. *Phys. Chem. Chem. Phys.* **2002**, *4* (12), 2747−2753.
(33) Kamitsos, E. I.; Tzinis, C. H.; Risen, W. M. Raman Study of the Mechanism of Electrical Switching in Cu TCNQ Films. *Solid State Commun.* **1982**, *42* (8), 561−565.
(34) Xiao, K.; Tao, J.; Pan, Z.; Puretzky, A. A.; Ivanov, I. N.; Pennycook, S. J.; Geohegan, D. B. Single-Crystal Organic Nanowires of Copper−Tetracyanoquinodimethane: Synthesis, Patterning, Characterization, and Device Applications. *Angew. Chem., Int. Ed.* **2007**, *46* (15), 2650−2654.

DOI: 10.1021/acsami.7b01664
ACS Appl. Mater. Interfaces 2017, 9, 17271−17278